行政院國家科學委員會專題研究計畫成果報告

超快光學與超快光電子學之研究—子計劃一:次皮秒電脈衝與THz電訊號之產生、傳輸與量測之研究

Generation, Propagation and Diagnostics of Subpicosecond Electrical pulses and THz signals

計畫編號：NSC 87-2215-E-009-005
執行期限：86年08月01日至87年07月31日
主持人：潘犀靈　　國立交通大學光電工程研究所

一、中文摘要

本年度計畫成果摘要包括下列幾項:

1. 同步的時域偵測與雷射時序紊亂度的抑制

我們在鎖相迴路中利用皮秒電脈衝驅動光電諧波混頻器以達到同步偵測, 並可將雷射的相位雜訊降低兩個數量級

2. 觀察以三層扭曲量子阱飽和布拉格反射體(SSBR)產生飛秒脈衝的特性

我們觀察 SSBR 的超低飽和強度並在忽略克爾透鏡效應的情形下觀察有 SSBR 下鈦藍寶石雷射的啟動動力學

3. 觀察扭曲式量子阱飽和布拉格反射體(SSBR)的強大非線性現象與超快載子動力學

我們報導SSBR的暫態反射率可到4%．並在多波長的情況下展現載子動態力學的特性

4. 在漸寬增益區半導體雷射放大器的次皮秒脈衝光放大

我們報導在漸寬增益區半導體雷射放大器的非秒脈衝放大,最大增益可到14倍而最小的脈衝寬度可到267fs．更進一步我們展現在驅動電流接近閥值電流時的放大輸出可到68%, 而在雷射驅動電流接近1.65倍的閥值電流時便驟降到到10%

5. 利用液晶空間光調制器產生數位可調半導體雷射

具有窄線寬,數位可調波長之雷射輸出已經獲得;此雷射採用一種摺疊望遠鏡式的光柵,外腔為一液晶空間光反射器.

關鍵詞：雷射時序紊亂度、扭曲式量子阱飽和布拉格反射體(SSBR) 、啟動動力學、超快載子動力學、漸寬增益區半導體雷射放大器、液晶空間光調制器

Abstract

The abstract of this project report contain those items as following:

1. Simultaneous time-domain detection and suppression of laser timing jitter

We employ an optoelectronic harmonic mixer, biased by picosecond electrical pulses, in a phase-locked loop for simultaneous detection and suppression of laser phase noise by two orders of magnitudes.

2. Characterization of a triple strained-quantum-well saturable Bragg reflector (SSBR) for the generation of femtosecond pulses

We characterized the SSBR with ultra-low saturation fluence and the build-up dynamics of a Ti: sapphire laser with the SSBR and negligible Kerr-lens strength.

3. Giant Optical Nonlinearity and Ultrafast

Carrier Dynamics of a Strained Quantum Well Saturable Bragg Reflector (SSBR)

We report normalized nolinear reflectivity as large as 4% for a SSBR. Experiments were performed at multiple wavelengths to elucidate carrier dynamics.

4. Subpicosecond Pulse Amplification In a Tapered-waveguide Laser Diode Amplifier

Femtosecond pulses amplification in a tapered-waveguide laser diode amplifier with a maximum gain of 14 and minimum output pulse width of 267 fs is reported. Further, we show that the percentage of the amplified output that is ultrafast is about 68% at $I \sim I_{th}$ and rapidly decreased to 10% for $I \sim 1.65\ I_{th}$.

5. Digitally Tunable Laser Diode With a Liquid Crystal Spatial Light Reflector

Narrow-linewidth, digitally wavelength-tunable output is obtained by a laser diode with an external folded telescopic grating loaded external cavity incorporating a liquid spatial light reflector (LC-SLR).

Keywords: laser timing jitter, Strained Quantum Well Saturable Bragg Reflector (SSBR), build-up dynamics , Ultrafast Carrier Dynamics, Tapered-waveguide Laser Diode Amplifier, Liquid Crystal Spatial Light Reflector(LC-SLM)

二、內容

1. **Simultaneous time-domain detection and suppression of laser timing jitter**

緣由與目的

Phase noise or timing jitter is an important attribute of mode-locked lasers. Active laser timing stabilization or synchronization schemes are often required in applications [1]. In this work, we demonstrate a new phase stabilization technique that allows us to phase-lock up to the 33rd laser harmonic component. Simultaneous detection of phase noise for determination of laser timing jitter is also achieved in lieu of the use of commercial vector signal analyzers as in the recent work of Tsuchida [2]

結果與討論

Our experimental setup is shown in Fig. 1. The laser was a femtosecond passively mode-locked Ti:sapphire laser with a strained saturable Bragg Reflector (SSBR) [3]. The key component in our phase detection and suppression scheme is a GaAa:Cr photoconductive switch that acts as the optoelectronic harmonic mixer (OEHM). It is used for intermixing the harmonics of the laser pulse train at f_o and harmonics of the RF signal from a comb generator (f = 1000 MHz) to generate an intermediate frequency (IF) signal at 150 kHz ($f_{IF} = Nf - Mf_o$). For the phase noise detection part of this scheme, the IF signal is fed to a digital phase comparator where it is compared in phase with a synchronous reference signal (f_R = 10 MHz) through a frequency divider. The error signal generated from the digital phase comparator was then fed to a 12-bit A-D card. After signal processing using FFT algorithms, the phase noise spectrum could be obtained. For comparison, conventional power spectral analysis is also performed.

The timing jitter of the laser without active phase control was determined by conventional power spectral measurements to be above 7.5 ps and up to several tens of picoseconds by deliberately adjusting the

intracavity bandwidth. The single-sideband (SSB) phase-noise spectrum of the stabilized laser is shown in Fig. 2. For this case, the 3rd-harmonics of the RF signal was intermixed with the 33th-harmonics of the laser pulse train. The corresponding RMS timing jitter is 662fs (100-500Hz) and 661fs (0.5-5kHz), respectively. The error signal taken from the digital phase comparator sampled at 10 kHz in 0.5 sec is shown in the inset of Fig.2, which indicates a time-averaged timing fluctuation of about 0.35ps. After performing FFT on the phase-noise data, we determined that the RMS timing jitter of the stabilized laser is 254fs (100-500Hz) and 236fs (0.5-5kHz), respectively. The discrepancy is due to (1) the frequency domain approach is valid for active mode-locked laser for which the central frequency of laser pulse train is quasi-stationary; and (2) amplitude noise that can not be subtracted out completely in the power spectral analysis. In Fig. 3, we show frequency- and time-domain results of SSB phase noise spectral density for the stabilized laser by locking the 11th, 22nd, and 33rd laser harmonics. The timing jitter decreased with the use of higher harmonics as expected. On the other hand, the time-domain jitter data are consistently two times smaller than those from the conventional spectral analysis.

In summary, we show a new technique which can be used to stabilize the laser at high harmonics by extending the fundamental RF signal frequency via a comb generator. The same scheme also provides the time domain phase noise detection capability. This work was supported in part by the National Science Council of the Republic of China.

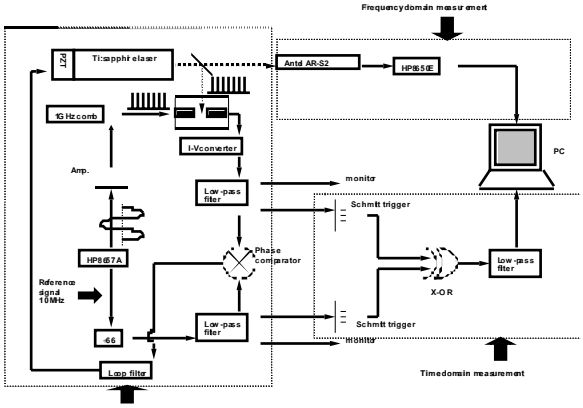

Fig.1 Schematic diagram of the high harmonic OEPLL for active timing stabilization and time domain phase noise Measurement

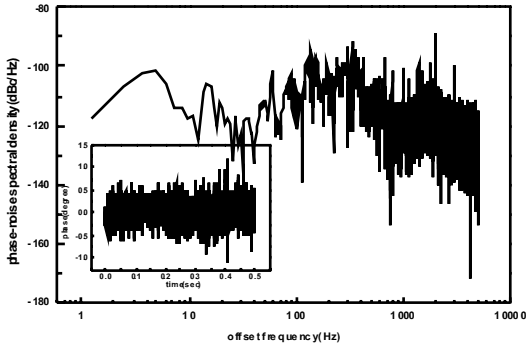

Fig.2 Single-sideband phase-noise spectral density for the stabilized laser and harmonic of RF signal by conventional frequency domain approach.

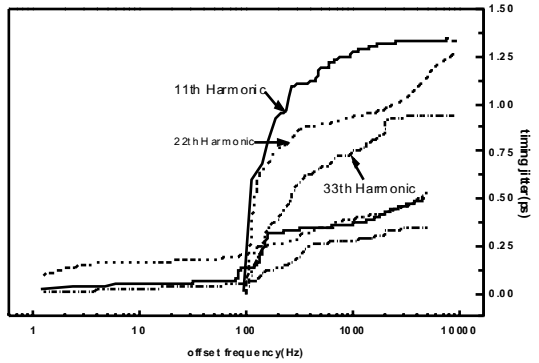

Fig.3 Single-sideband phase-noise spectral density for the stabilized laser by time domain approach.

2. Characterization of a triple strained-quantum-well saturable Bragg reflector (SSBR) for the generation of femtosecond pulses

緣由與目的

Lately, there have been substantial interests in passively mode-locked solid state lasers with semiconductor saturable absorber mirror

(SESAM) [4,5]. Pulses as short as 6.5 fs were generated. In this work, the saturation fluence of a new type of SESAM, the triple strained-quantum-well Bragg reflector (SSBR) [6] was determined by ultrafast nonlinear reflectivity measurements. The ultra-low saturation fluence are consistent with wavelength-dependent buildup dynamics of the laser with the SSBR and negligible Kerr-lens-mode-locking (KLM) strength. Such lasers are capable of sustaining stable sub-100fs pulses.

結果與討論

The laser configuration with a triple strained-quantum-well saturable Bragg reflector (SSBR) and weak KLM has been described previously [6]. The structure, reflection and continuous wave photoluminescence (PL) spectra are shown in Fig. 1, 2. The output power and pulse width of the Ti : sapphire/SSBR lasers pumped by an argon laser at 5W were 230 mW and 90 fs respectively. Using pump-probe techniques, we have determined the normalized nonlinear reflectivity $\Delta R/R$ as a function of average power (P_{inc}) incident on the SSBR at several wavelengths in the tuning range of mode-locked laser with this SSBR device (see Fig. 3). From Fig. 3, We find that the saturation optical fluence E_{sat} were all about $12\mu J/cm^2$ (P_{inc} ~ 40mW). This is explained by noting that they are associated with the same exciton absorption resonance. On the other hand, the linear absorption strength decreased as the wavelength was shifted away from the peak absorption wavelength (λ = 755 nm). This trend was also observed in PL measurements.

The transient second harmonic signal for this laser during the buildup are shown in Fig. 4. The wavelengths of the laser was set at λ = 775nm, 786nm, and 795nm for the buildup experiment. Figure 5 showed the corresponding theoretical buildup trace obtained using the master equation approach with KLM neglected. In separate experiments, we have determined that the unsaturated loss q_o, the fast decay time and the slow decay time of the SSBR are 0.6 ~ 3×10^{-3}, 280 fs and 40 ps respectively (The beam spot size on SSBR ≈ 100μm). The theoretical and experimental results are in excellent agreements. The CW stage and total buildup time were 60 us and 100 us atλ = 775nm. At λ =786nm, these values lengthened to ~65us and 150us. The relatively drastic change of in these time scales can be explained by the decrease of rapid recovery of saturation effect. The nonlinear reflectivity traces at the three wavelengths shown in Fig. 6 could identify this. For $\lambda = 795nm$, the corresponding time scales were ~100us and 210us. This can be explaiend by the weaker linear absorption strength of the SSBR at the longer wavelength. Since the KLM mechanism was neglected in our simulation, our results indicate that the laser with SSBR could generate stable sub-100 fs pulse without the aid of the KLM mechanism.

In conclusion, nonlinear reflectivity measurements were performed to determine the saturation fluence of triple strained-quantum-Well SBR with ultralow saturation fluence of 12 $\mu J/cm^2$ by studying time-resolved nonlinear reflectivity and pulse-forming dynamics. Studying of the buildup dynamics demonstrated that mode-locking force of SSBR could self-start and stabilize the sub-100 fs pulse forming.

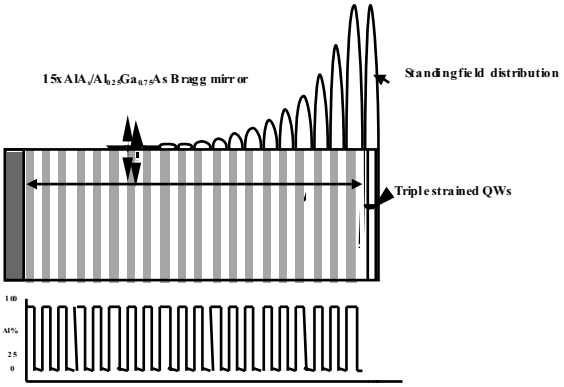

Fig.1. Structure of the strained-layer saturable Bragg reflector (SSBR) with a distributed Bragg reflect (DBR) and an additional λ/2 layer of $Al_{0.25}Ga_{0.75}As$; three quantum wells with different absorption peak were inserted in this layer.

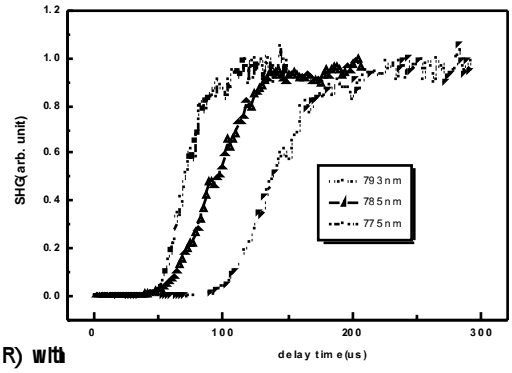

Fig.4. The experimental transient second harmonic signal for three

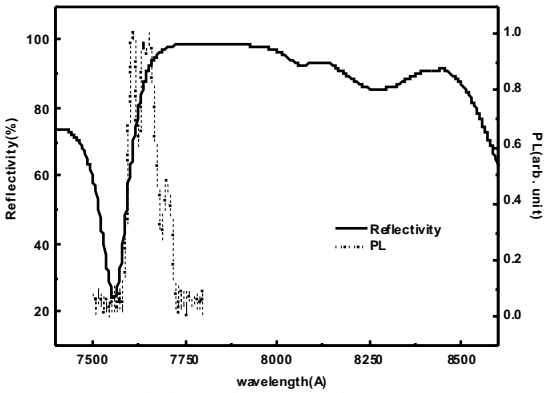

Fig.2. The reflectivity and the CW photo-luminescence (PL) spectra of the SSBR.

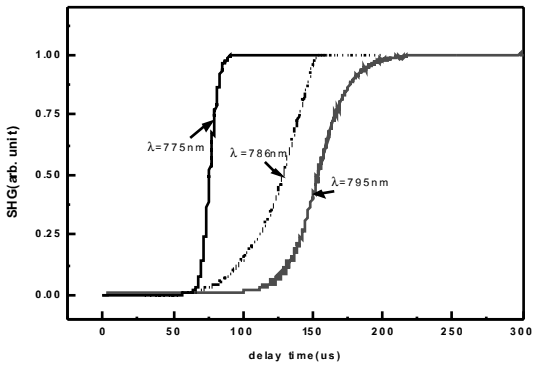

Fig.5 The theoretical transient second harmonic signal for three

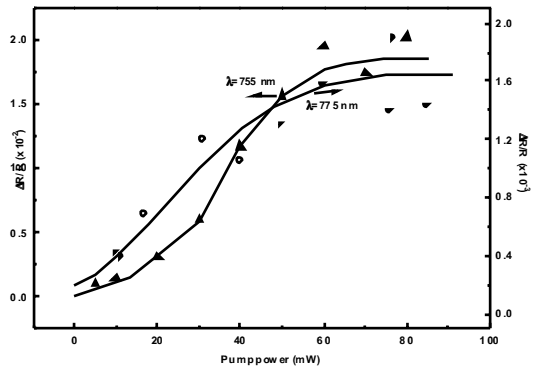

Fig.3. Normalized nonlinear reflectivity of the SSBR at λ = 755 nm and 775 nm are plotted as a function of incident average power.

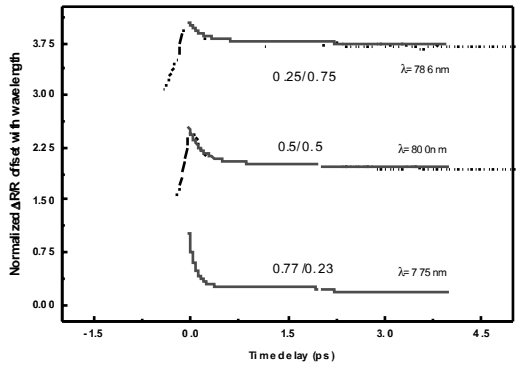

Fig.6 The nonlinear reflectivity trace and fitting curve of three wavelength. The fast/slow ratio of fitting curve are also shown.

3. Giant Optical Nonlinearity and Ultrafast Carrier Dynamics of a Strained Quantum Well Saturable Bragg Reflector (SSBR)

緣由與目的

Recently, semiconductor saturable Bragg reflectors (SBR's) have been successfully

developed for passive mode-locking of solid state lasers [7~9]. In particular, we have developed a triple strained quantum well saturable Bragg reflector (SSBR) with saturation fluence as low as 12 $\mu J/cm^2$ [10]. This suggests potential applications of this device for applications such as all-optical swiching and modulation. In this work, we report a new type of SBR using triple strained-layer quantum wells as the absorbing layer which named strained saturated bragg reflector(SSBR). Because of it`s low saturation energy and large tunning range, we want to understand the carrier dynamics with detailed wavelength. The time-resolved differention reflection (R/R) in this SSBR with detailed varient pumping energies have been observed. The influence of carrier scattering and process of recombination on the temperal and spectral R/R dynamics have been investigated.

結果與討論

The structure, reflectivity and photoluminescence spectra of the SSBR are shown in Fig. 1. Femtosecond pump/probe experiments were performed. The normalized time-resolved reflectivity, R/R, of the SSBR sample as a function of the pumping wavelength are shown in Fig. 2. The wavelength-dependent peak values of R/R are plotted in Fig. 3. When the sample was excited at a photon energy above the band gap (. < 757.5nm) , R/R is positive and with a peak value of (~4%) at 755nm. It must be very large compared with other bulk material , like GaAs. The large optical nonlinearity can be attributed in part to band filling and reduced absorption. Further, the optical excitation of carriers induced charges screening the internal piezoelectric field. This leads to absrption bleaching and can result in very large optical nonlinearities.[11] There have a large peak magnitude of the transient R/R in 755nm and negative sign from 760nm. This anomalous dispersion trend had been demonstrated in other papers[12] From 755nm to 760nm, the ratio of the peak negative value to the positive value of R/R increased and then decreased from 760nm to 775nm. A sign reversal for R/R with peak negative magnitude of -0.6% was observed at 760nm. This can be explained by using the free carrier absorption model. By analyzing the transient R/R signal, we also determined that the fast and slow carrier lifetimes of the SSBR. The wavelength dependence are shown in Fig. 4(a) and (b). While the wavelength dependence for the fast component of the carrier lifetime is not apparent, the slower component decreased by about an order of magnitude from 250 ps at 750 nm to 20 ps at 775 nm.

In summary, normalized nolinear reflectivity as large as, 4% at 755nm was observed and attributed to band filling, screening effect and surface field enhancement effects. Sign reversal of the transient R/R signal from 760nm to 775nm are explained by the free carrier absorption effect. The wavelength-dependence of the fast and slow components of the carrier lifetime is significant for the performance of the SSBR as an effective saturable absorber for stable mode-locking.

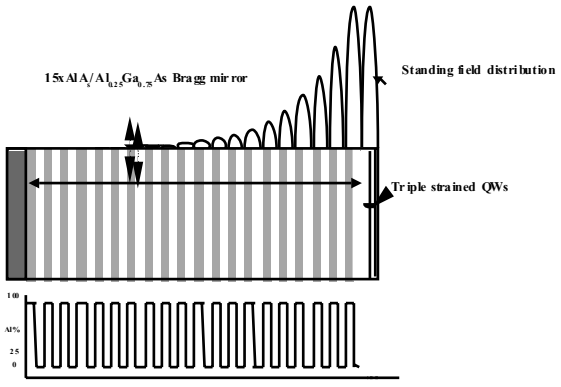

(a)

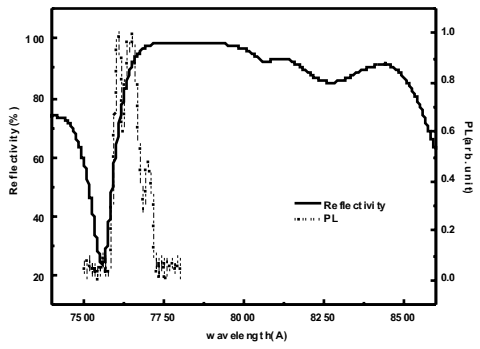

(b)

Fig. 1 (a) Structure of the strained-layer saturable Bragg reflector (SSBR) with a distributed Bragg reflect (DBR) and an additional $\lambda/2$ layer of $Al_{0.25}Ga_{0.75}As$; three quantum well with different absorption peak were inserted in this layer.

(b) The reflectivity and the CW photo-luminescence (PL) spectra of the SSBR

(a)

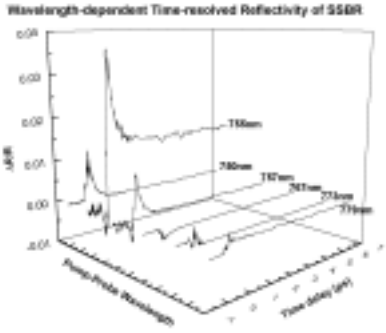

Fig.2 Wavelength-dependent time-resolved reflectivity of SSBR

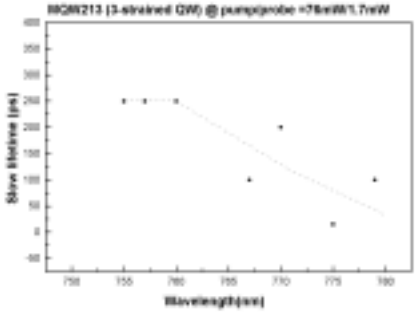

(b)

Fig. 4 The dependence of (a) fast and (b) slow carrier lifetime with pumping wavelength

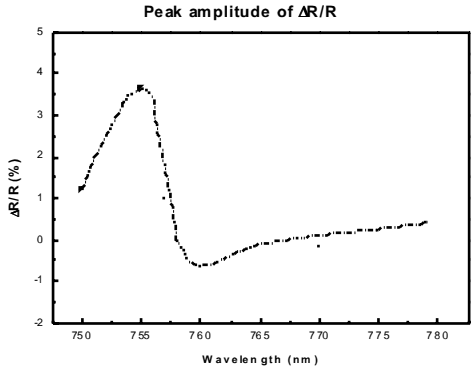

Fig. 3 The peak amplitude of ΔR/R at different pumping wavelength

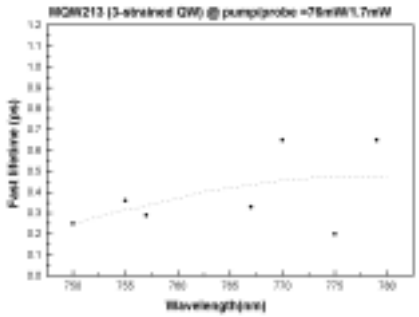

4. Subpicosecond Pulse Amplification In a Tapered-waveguide Laser Diode Amplifier

緣由與目的

Ultrashort pulse amplification in laser diode amplifiers (LDA's) has attracted considerable attention because of its potential applications in optical communication and signal processing. With the advent of LDA's with tapered-waveguide, several groups have investigated both experimentally and

theoretically the prospect of generating high-power picosecond pulses using such devices [13-16]. In this paper, we report the first subpicosecond pulse amplification experiment in LDA's with tapered-waveguide (TW-LDA).

結果與討論

We perform our experiments with a home-made passively mode-locked Ti: sapphire/SBR laser. Transform-limited 150 fs pulses (λ = 812 nm) at 82 MHz were injected into a one-side AR-coated tapered-waveguide diode chip found in a commercial tunable diode laser, SDL-8630. The amplified pulses were analyzed with an intensity autocorrelator and optical spectrum analyzer.

Figure 1 depict autocorrelation traces of the transmitted pulses at the output of the TW-LDA as a function of the dc bias current ($0.82I_{th} \le I \le 1.64\, I_{th}$, I_{th} = 450 mA). The pulse shape is Gaussian while the FWHM gradually increases from 260 fs to 440 fs at I = 1.6 A. For $I \le I_{th}$, the output bandwidth is nearly transform-limited with a spectral bandwidth of 4 – 5 nm. Near threshold, this rapidly decreased to 2.2 nm and approaches 1.8 nm at $I \sim I \le 1.64\, I_{th}$. Significant rise of the baseline of the autocorrelation traces for $I \ge I_{th}$ is also evident in Fig. 1. The output then corresponds to perfectly phase-locked components with a broad tail consisting of partially phase-locked and randomly-phased modes. In Fig. 2, we have plotted the inverse contrast ratio, R^{-1}, of the LDA-TW output correlation traces as a function of I/I_{th}. We define R as the peak-to-shoulder value of the autocorrelation traces. Thus R^{-1} =0 for perfectly phase-locked pulse and R^{-1} = 0.5 for randomly phase modes. Also plotted in Fig. 2 is the fractional energy, β, which is defined as $\beta = \frac{E_p}{E_{total}}$, where E_p is the energy of the pulse and E_{total} is the energy of pulse with background. It can be calculated from the SHG conversion efficiency as we described previously. [17] Below I_{th}, $R^{-1} \sim 0$ while β is nearly 100%. These two parameters changed drastically near I_{th}, e.g. $\beta \sim 68\%$ or 68% of the pulse energy is within the femtosecond phase-locked pulse. For $I \sim 1.6\, I_{th}$, β reduced to 10% while $R^{-1} \sim 0.4$. That is, most of the pulse energy is within the partially phase-locked or randomly phase-locked modes. In Fig. 3, we have plotted gain of the LDA-TW as a function of bias current. The maximum observed gain at I/I_{th} was nearly 14dB.

In summary, we report first experimental results of subpicosecond pulse amplification in tapered-waveguide laser diode amplifiers. We are also able to determine for the first time fraction of the amplified output that is ultrafast.

Acknowledgements: This work was partially supported by the National Science Council of the R.O.C. under various grants.

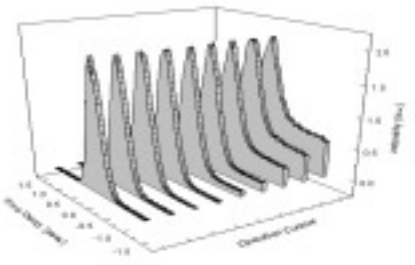

Fig. 1 Autocorrelation traces of the subpicosecond amplified pulses as a function of bias current.

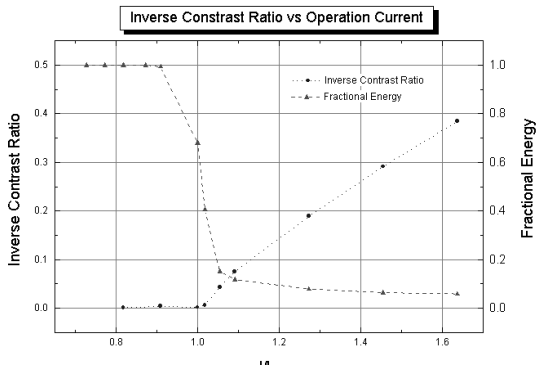

Fig. 2 Inverse contrast ratio and fractional energy of the subpicosecond amplified pulses as a function of bias current

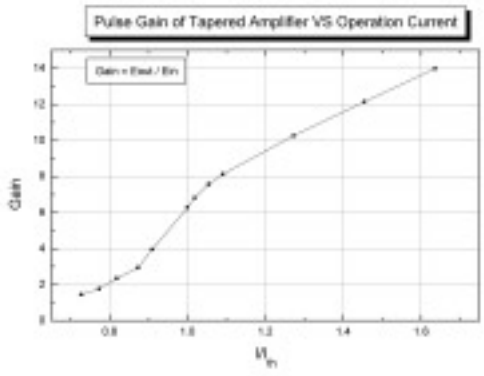

Fig. 3 Pulse gain of the tapered amplifier as a function of bias current.

5. Digitally Tunable Laser Diode With a Liquid Crystal Spatial Light Reflector

緣由與目的

Owing to their applications in coherent optical communication, high-resolution spectroscopy and optical metrology, tunable external cavity semiconductor lasers have been extensively studied in the past decade. Typical tuning methods employ bulk and fiber-type Littrow and grazing-incidence gratings, Fabry-Perot Eaton or interference filter, as well as electro-optic or acousto-optic tunable filter [18]. In this work, we report a novel digitally wavelength-tunable laser diode by using a folded telescopic grazing-incidence grating-loaded external cavity [19] incorporating a liquid crystal spatial light reflector.

結果與討論

A schematic of the laser is shown in Fig. 1. A low-power red laser diode (LD, $\lambda = 650$ nm) from a commercial laser pointer was used without modification. Output of the LD was collimated and incident on the grating (1800 lines/mm) at an angle of 79°. The primary laser output is the zeroth-order reflection of the grating (~ 60% of the incident light from the diode chip). The first-order-diffracted light was collected by a lens and focused on the LC-SLR. That is, a reflection-mode spatial light modulator as shown in Fig. 2. It is based on the design of a normally off twisted nematic liquid crystal (NLC) cell. A 6-μm-thick NLC (E7 manufactured by Merck) layer was sandwiched between a glass cell with indium-tin-oxide (ITO) electrodes. One of the ITO-electrodes was patterned. The pattern consisted of fifty 100 μm × 2 cm stripes with 5 μm spacing. The polarizer was aligned to transmit light parallel to that of the incident laser polarization. The back mirror was an Au-coated silicon substrate. Narrow-band laser oscillation at the desired wavelength is achieved by optical feedback of the retro-reflected light from one pixel of the LC-SLR, which was electrically biased, to the laser diode. The width of the pixel was chosen such that only one mode of the bare diode chip was selected. The laser is digitally tunable by electrically biasing the individual pixels, with wavelength steps $\Delta\lambda$ determined by center-to-center separation of the adjacent pixels Δx. That is,

$$\Delta\lambda = \Lambda \cos\theta_r \Delta x / f, \quad (1)$$

where Λ is the grating period; θ_r is the first-order diffraction angle; f is the focal length of the lens.

The contrast ratio of the homemade

LC-SLR is about 5:1. Because of high gain of the semiconductor media, the LC-SLR can achieve the desired spectral filtering function. The threshold switching voltage of the LC-SLR is 4 V_{pp} (peak -to – peak) at 10 kHz. Complete switching from off- to on-state is achieved at 10V_{pp}. The switching time is ~ 175 ms, which is determined by the characteristics of the twisted NLC cell.

Figure 3 illustrate the narrow-band (< 0.2 nm, instrument limited) output of the laser as measured by an optical spectrum analyzer (Anritzu, model MS9030). The laser wavelength can be tuned from 636 to 643 nm discretely in 0.27 nm steps by biasing sequentially the pixels. The side-mode-suppression-ratio (SMSR) of the laser was better than 20 dB throughout this range. In Fig. 4, we plot the lasing wavelength as a function of the pixel number. It is in good agreement with the theoretical prediction according to Eq. (1). The wavelength resettability of the present laser is excellent. After switching to a different pixel, the laser wavelength is reset. Realignment of the laser cavity is not necessary. The tuning range of the laser is limited by the reflectivity of the front facet of the LD. With anti-reflection coating such that R < 1% for this facet, the tuning range of the laser can easily exceed several tens of namometers [19]. The SMSR of the laser output can be improved if we employ LC-SLR's with higher contrast ratios.

In summary, we demonstrate a novel digitally tunable laser diode. This is realized by using a folded telescopic grating-loaded external cavity with a LC-SLR at the focal plane of the folded telescope. To demonstrate, we achieved narrow-band tunable output from 636 to 643 nm in 0.27 nm steps with a low-power red LD in a commercial laser pointer. The SMSR of the laser output was better than 20 dB throughout this range. The tuning range and SMSR is limited by the reflectivity of the front facet of the LD and contrast ratio of the LC-SLR. The wavelength switching time was ~ 175 ms.

Acknowledgement: This work was partially supported by the National Science Council of the R.O.O. under various grants.

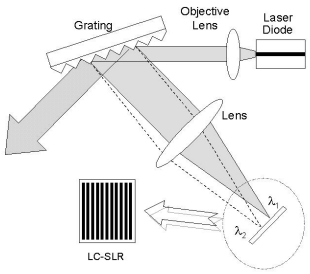

Fig.1

Fig. 1 A schematic of the digitally tunable laser. LC-SLR: Liquid Crystal Spatial Light Reflector.

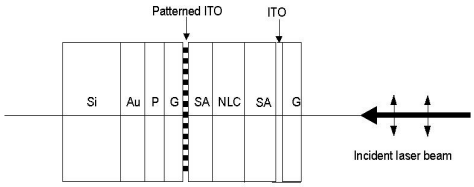

Fig.2

Fig. 2 Configuration of the LC-SLR. G: glass plate; ITO: indium-tin-oxide coating; NLC: nematic liquid crystal; SA: surface alignment layer; P: polarizer; Au: evaporated gold coating; Si: silicon substrate.

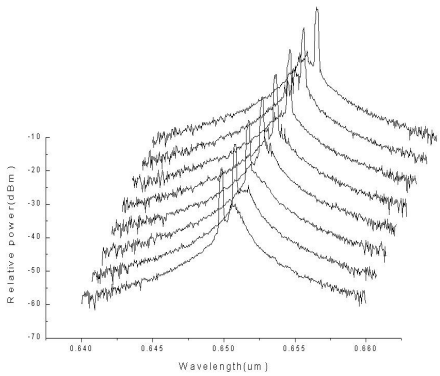

Fig.3

Fig. 3 Narrow-linewidth output spectra of the tunable laser diode.

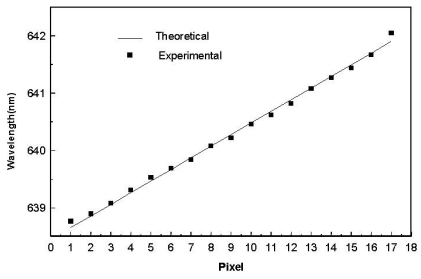

Fig.4

Fig. 4 Lasing wavelength as a Function of the pixel number. The solid line is the theoretical curve. The solid squares are experimental data.

三、參考文獻

References

1. Jia-Min Shieh, Shang-Cheng Liu and Ci-Ling Pan, J. Opt. Soc. Am. B**15**, 1802 (1998).
2. Hidemi Tsuchida, Opt. Lett. **23**, 286 (1998)
3. Jia-Min Shieh, T. C. Huang, K. F. Huang, Chi-Luen Wang, and Ci-Ling Pan, *Optics Communications,* **156**(1-3), 53 (1998).
4. S. Tsuda, W. H. Knox, S. T. Cundiff, W. Y. Jan, and J. E. Cunninjham, IEEE Sel. Topics Quantum Electron. 2, 454.(1996).
5. U. Keller, K. J. Weingarten, F. X. Kartner, D. Kopf, B. Braun, I. D. Jung, R. Fluck, C. Honninger, N. Matuschek, and J. A. der Au, IEEE J. Sel. Topics Quantum Electron. 2, 435 (1996).
6. Jia-Min Shieh, T. C. Huang, K. F. Huang, Chi-Luen Wang, and Ci-Ling Pan, Optics Comm., 156, 53 (1998) .
7. S.Tsuda et al, IEEE Sel. Topics Quantum Electron. 2, 454 (1996).
8. M. J. Hayduk et al, Optics Comm., 137,55 (1997)
9. U. Keller et al, IEEE J. Sel.Topics Quantum Electron. 2, 435 (1996).
10. . Jia-Min Shieh, T. C. Huang, K. F. Huang, Chi-Luen Wang, and Ci-Ling Pan, Optics Communications, 156(1-3), 53 (1998).
11. D. L. Smith and C. Mailhiot, Phys. Rev. Lett. 58,1264, 1987.
12. B. R. Bennet et al, IEEE J. Quantum Electron, 26, 113, 1990.
13. H. Ghafour-Shiraz, Pen Wei Tan, and T. Aruga, "Picosecond Pulse Amplification in Tapered-Waveguide Laser-diode Amplifiers," IEEE J. Sel. Topics in Quantum Electron., vol. 3, no. 2, pp. 210-217, 1997.
14. B. Dagens, S. Balsamo, and I. Montrosset, "Picosecond Pulse Amplification in AlGaAs flared Amplifiers," ibid., pp. 233-244, 1997.
15. A. Mar, R. Helkey, J. Bowers, D. Mehuys, and D. Welch, "High Power Mode-Locked Compound Laser Using a Tapered Semiconductor Amplifier," IEEE Photonics Technol. Lett., vol. 6, No. 9, pp. 1070-1072, 1994.
16. L. Goldberg, D. Mehuys, and D. Welch, "High Power Mode-Locked Compound Laser Using a Tapered Semiconductor Amplifier," ibid., pp. 1070-1072, 1994.
17. Jia-Min Shieh, Hwa-Ming Twu, and Ci-Ling Pan, "Effects of intracavity dispersion on the starting dynamics of continuous-wave passively mode-locked Ti:sapphire/DDI lasers," Opt. Lett.,

Vol.21, No.14 1058-1060 (1996)
18. . P. Zorabedian, "Tunable External-Cavity Semiconductor Lasers," in F. J. Duarte, ed., Tunable Lasers Handbook, 1995, Academic Press, San Diego, Chapter 8.
19. Ci-Ling Pan and Chi-Luen Wang, Opt. Quantum Electron. Vol. 28, pp. 1239 – 1257, 1996. And references therein.